MCB
Journals.ASM.org

Essential Function of Protein 4.1G in Targeting of Membrane Protein Palmitoylated 6 into Schmidt-Lanterman Incisures in Myelinated Nerves

Nobuo Terada,[a,b] Yurika Saitoh,[a] Nobuhiko Ohno,[a] Masayuki Komada,[c] Sei Saitoh,[a] Elior Peles,[d] and Shinichi Ohno[a]

Department of Anatomy & Molecular Histology, Interdisciplinary Graduate School of Medicine and Engineering, University of Yamanashi, Chuo City, Yamanashi, Japan[a]; Department of Occupational Therapy, School of Health Sciences, Shinshu University School of Medicine, Matsumoto City, Nagano, Japan[b]; Department of Biological Sciences, Tokyo Institute of Technology, Yokohama City, Kanagawa, Japan[c]; and Department of Molecular Cell Biology, Weizmann Institute of Science, Rehovot, Israel[d]

Protein 4.1G is a membrane skeletal protein found in specific subcellular structures in myelinated Schwann cells and seminiferous tubules. Here, we show that in the mouse sciatic nerve, protein 4.1G colocalized at Schmidt-Lanterman incisures (SLI) and the paranodes with a member of the membrane-associated guanylate kinase (MAGUK) family, membrane protein palmitoylated 6 (MPP6). Coimmunoprecipitation experiments revealed that MPP6 was interacting with protein 4.1G. In contrast to wild-type nerves, in 4.1G knockout mice, MPP6 was found largely in the cytoplasm near Schwann cell nuclei, indicating an abnormal protein transport. Although the SLI remained in the 4.1G knockout sciatic nerves, as confirmed by E-cadherin immunostaining, their shape was altered in aged 4.1G knockout nerves compared to their shape in wild-type nerves. In the seminiferous tubules, MPP6 was localized similarly to protein 4.1G along cell membranes of the spermatogonium and early spermatocytes. However, in contrast to myelinated peripheral nerves, the specific localization of MPP6 in the seminiferous tubules was unaltered in the absence of protein 4.1G. These results indicate that 4.1G has a specific role in the targeting of MPP6 to the SLI and the assembly of these subcellular structures.

Protein 4.1G (4.1G) is a member of the 4.1 family (27, 46), a group of membrane skeletal proteins that link various components to the spectrin-actin network (10). We have previously reported that 4.1G is present in rodent Schwann cells (7, 24) and mouse seminiferous tubules (40, 41). In peripheral nerves, 4.1G is found at the Schmidt-Lanterman incisures (SLI) and the paranodal loops of myelinated Schwann cells (24). The SLI are funnel-shaped interruptions within the myelin sheath of nerve fibers. They contain high concentrations of actin and spectrin (35, 42), which forms a membrane skeleton that might contribute to the elasticity and stability of these structures.

Membrane-associated guanylate kinase (MAGUK) family proteins contain PDZ (for postsynaptic density 95 [PSD-95]/*Drosophila* disks large [Dlg]/zonula occludens 1 [ZO-1]), GUK (guanylate kinase), and SH3 (src homology 3) domains, and they localize to specific domains at the plasma membranes (9, 11). In epithelial cells, for example, some MAGUKs, such as Dlg and ZO-1, are required for the formation of adherens and tight junctions, respectively. In addition to their function as membrane scaffolds (16, 21), several MAGUKs also control intracellular protein transport through their ability to bind motor proteins (45, 49). Interestingly, some MAGUKs contain specific domains that interact with 4.1 proteins (14, 17, 18). In the current study, we report the identification of membrane protein palmitoylated 6 (MPP6) (also known as PALS2, VAM1, and p55T [http://www.genenames.org/]) as a novel MAGUK molecule that interacts with 4.1G in peripheral nerves. We further demonstrate that the interaction between 4.1G and MPP6 is essential for the targeting of the latter into SLI.

MATERIALS AND METHODS

Animals and anesthesia. All animal experiments were performed in accordance with the guidelines of the Animal Care and Use Committee of the University of Yamanashi. The production of the $4.1G^{-/-}$ (37) and $4.1B^{-/-}$ (23) mice was previously described. Adult (10-month-old) wild type, $4.1G^{-/-}$, $4.1B^{-/-}$, and double-knockout $4.1G^{-/-}/B^{-/-}$ mice (n = 6 mice for each genotype) were anesthetized with pentobarbital and processed for the following preparation procedures.

IVCT for living mouse sciatic nerves and subsequent FS. An *in vivo* cryotechnique (IVCT) was performed on the exposed sciatic nerves of the anesthetized mice by directly pouring 50 ml liquid isopentane-propane cryogen (−193°C) cooled in liquid nitrogen, as previously described (38). The frozen nerves were removed with a dental electric drill in liquid nitrogen and processed for routine freeze-substitution fixation (FS) in acetone containing 2% paraformaldehyde at −80°C for 24 h and then at −30, −10, 4°C, and room temperature (RT) for 2 h each, as described previously (41). They were washed in pure acetone and xylene and embedded in paraffin.

Perfusion fixation followed by teasing for sciatic nerves or sucrose embedding for testes. To obtain perfusion-fixed sciatic nerves or testes, anesthetized mice were perfused with 2% paraformaldehyde in 0.1 M phosphate buffer (PB; pH 7.4) via the heart. The sciatic nerves or testes then were removed and immersed in the same fixative at 4°C for 2 h. To produce teased nerve fibers, the fixed sciatic nerves were separated with fine needles under a stereomicroscope and frozen with isopentane precooled in dry ice. The frozen nerves then were thawed in phosphate-buffered saline (PBS; pH 7.4) at RT, freeze-thawed again, and then used for the immunostaining. For some teased sciatic nerves, the freeze-thaw treatment was not performed, and heights of the SLI circular truncated cones with immunostaining and phalloidin staining, described in the next

Received 15 July 2011 Revised 3 August 2011 Accepted 18 October 2011
Published ahead of print 24 October 2011
Address correspondence to Nobuo Terada, nobuot@shinshu-u.ac.jp.

doi:10.1128/MCB.05945-11

section, were measured. Testes were rinsed in PBS, immersed in 30% sucrose-5% glycerol in PB at 4°C overnight, embedded in optimum-cutting-temperature (OCT) compound (Tissue-Tek; Sakura Finetechnical, Tokyo, Japan), and frozen with isopentane precooled in dry ice.

Immunostaining and phalloidin staining for light microscopic observation. For paraffin-embedded IVCT-FS sciatic nerves, 4-μm-thick sections were cut, routinely deparaffinized with xylene, and infiltrated in a graded series of ethanol and PBS. For sucrose-embedded frozen testis tissues, 6- to 8-μm-thick cryosections were cut in a cryostat machine and infiltrated into PBS. Some deparaffinized sections were stained with hematoxylin-eosin (HE) for pure morphology at the light microscopic level. For common immunostaining, sections were pretreated with hydrogen peroxide and normal goat serum, followed by rabbit polyclonal anti-MPP6 antibody (Ab) (Sigma, St. Louis, MO), anti-4.1G Ab (ProteinExpress, Kisarazu, Ibaraki, Japan), or rat monoclonal anti-E-cadherin Ab (Takara BioInc., Ohtsu, Shiga, Japan) at 4°C overnight. They were treated with biotinylated anti-rabbit or anti-rat IgG Abs (Vector, Burlingame, CA) at RT for 1 h and then with a horseradish peroxidase-labeled avidin-biotin complex (ThermoSci, Rockford, IL) at RT for 1 h, and they were visualized with a metal-enhanced diaminobenzidine (DAB) method (ThermoSci). Finally, they were incubated in 0.04% osmium tetroxide solution for 30 to 60 s and observed under a light microscope. Staining with only the secondary anti-rabbit or anti-rat IgG antibody was used as the control.

For double immunofluorescence staining for MPP6 and E-cadherin, the teased sciatic nerves were treated with PBS containing 0.1% Triton X-100 (PBS-T) at RT for 2 h and incubated with both rabbit polyclonal anti-MPP6 (Sigma) and rat monoclonal anti-E-cadherin (Takara) Abs at the same time in PBS-T at 4°C overnight. They were treated with Alexa Fluor 488-conjugated anti-rabbit IgG and Alexa Fluor 594-conjugated anti-rat IgG Abs (Invitrogen, Carlsbad, CA) at RT for 1 h.

For fluorescence double staining for E-cadherin and filamentous actin, teased sciatic nerves were incubated with Alexa Fluor 488-conjugated phalloidin (Invitrogen) and rat anti-E-cadherin Ab at the same time in PBS-T at 4°C overnight. They were treated with Alexa Fluor 594-conjugated anti-rat IgG Ab (Invitrogen) at RT for 1 h.

They were observed under a fluorescence microscope (FM) or confocal laser-scanning microscope (CLSM; FV1000; Olympus, Tokyo, Japan). The measurement of SLI circular truncated cone height with E-cadherin immunostaining and phalloidin staining was performed for 600 SLI in three $4.1G^{+/+}$ or $4.1G^{-/-}$ mice each. The *P* value was determined with Student's *t* test after evaluating their normal distribution.

Preembedding immunoelectron microscopy. Conventional preembedding immunoelectron microscopy was performed for the mouse testes as reported before (36). Briefly, anesthetized mice were perfused via their hearts with 2% paraformaldehyde in PB, and cryostat sections were produced and immunostained in the same way as that for the sucrose-embedded testis cryosections described in the previous section. After immunostaining, sections were fixed again with 0.25% glutaraldehyde in PB for 10 min and visualized by the DAB method. They then were additionally treated with 1% OsO_4 in PB for 20 min, dehydrated with a graded series of ethanol, and embedded in epoxy resin by the inverted gelatin capsule method. Ultrathin sections of 70-nm thickness were cut on an ultramicrotome and collected on copper grids. They were stained only with uranyl acetate and observed in an electron microscope (H-7500; Hitachi, Tokyo, Japan) at an accelerating voltage of 75 kV.

Immunoblotting and immunoprecipitation (IP) analyses. For immunoblotting, sciatic nerves of the $4.1G^{+/+}$ or $4.1G^{-/-}$ mice were immersed in Laemmli sample buffer, and the lysate protein concentration was adjusted by measurement with a protein assay kit (ThermoSci). Following SDS-PAGE, Western blotting was performed with an anti-MPP6 Ab. The blots were visualized using a chemiluminescence system (ThermoSci).

Immunoprecipitation analysis was performed for the adult $4.1G^{+/+}$ mouse sciatic nerves. To examine the 4.1G-MPP6 interactions, tissue lysates were obtained from the sciatic nerve supernatant by homogenization with a TENT buffer (20 mM Tris, pH 7.4, 1 mM EDTA, 50 mM NaCl, 1% Triton X-100) containing a protease inhibitor cocktail (Sigma) and centrifugation at 10,000 $\times$ *g* at 4°C for 30 min. The lysates were treated with protein G-Sepharose (GE Healthcare, Piscataway, NJ) at 4°C for 2 h to remove nonspecific proteins that were reactive to protein G, such as mouse IgGs. They then were incubated with a rabbit anti-MPP6 Ab that was the same as that for the immunohistochemistry experiments, rabbit anti-4.1G Ab (Bethyl Laboratory Inc., Montgomery, TX), or with rabbit IgG (Thermo Fisher Scientific, Cheshire, United Kingdom) at 4°C for 3 h. Immunoprecipitated molecular complexes were separated using protein G-Sepharose at 4°C for 2 h. All proteins were eluted from the Sepharose beads by boiling in Laemmli sample buffer and then subjected to SDS-PAGE and Western blotting analyses with the anti-4.1G Ab (ProteinExpress) or anti-MPP6 Ab.

RESULTS

Immunolocalization of MPP6 in sciatic nerves of wild-type and $4.1G^{-/-}$ sciatic nerves. In IVCT-FS samples of adult sciatic nerves, which preserve soluble proteins well in tissue sections (30), MPP6 immunoreactivity was detected in regions of noncompact myelin, including the SLI and the paranodes (Fig. 1A). Such localization is reminiscent of the one we previously reported for 4.1G (24). Given that 4.1 family proteins could bind to MPPs (22), we examined the expression of MPP6 in sciatic nerves isolated from mice lacking protein 4.1G (Fig. 1B). MPP6 was not detected in the SLI of $4.1G^{-/-}$ nerve fibers, and it was weakly observed in cytoplasm around nuclei of Schwann cells (Fig. 1B). However, similarly to wild-type nerves, MPP6 immunoreactivity still was detected in paranodes of $4.1G^{-/-}$ fibers (the bottom lane in Fig. 1B).

Since the localization and intensity of the MPP6 immunostaining was different in the $4.1G^{-/-}$ mice, we compared the total amounts of this protein between wild-type and $4.1G^{-/-}$ nerves by immunoblotting (Fig. 1C). As depicted in Fig. 1C, the amount of MPP6 in the $4.1G^{-/-}$ mice was markedly reduced compared to that in wild-type animals.

Molecular interaction of MPP6 with 4.1G. Using serial sections of sciatic nerves labeled for protein 4.1G and MPP6, we showed that both proteins colocalized at the SLIs (Fig. 2A). We next examined whether MPP6 and protein 4.1G interact in the sciatic nerve. Nerve lysates were prepared and subjected to immunoprecipitation with an antibody to MPP6 followed by immunoblotting with an antibody to protein 4.1G. As shown in Fig. 2B, protein 4.1G was specifically detected after immunoprecipitation with the anti-MPP6 antibody. Similarly, MPP6 was specifically detected after immunoprecipitating 4.1G from sciatic nerves (Fig. 2B). In contrast, neither MPP6 nor 4.1G was detected when the immunoprecipitation was carried out using a control rabbit IgG. Thus, both directional IP studies indicate that MPP6 and 4.1G interact in myelinating Schwann cells. These immunoprecipitation studies were repeated three times, and the blot lines were clearly detected each time.

Analysis of SLI in $4.1G^{-/-}$ sciatic nerve. To examine whether the reduced localization of MPP6 in the SLI reflects their abnormal formation, we compared the distribution of MPP6 to that of the known SLI protein E-cadherin (43) by using CLSM (Fig. 3A). By the accumulation of the Z-series optical sections ($4.1G^{+/+}$; Z-accum in Fig. 3A), the relationships among immunostained structures were recognized in wild-type nerves: MPP6 was immunolocalized at SLI, paranodes, and abaxonal and mesoaxonal membranes together with E-cadherin. In contrast, and in agree-

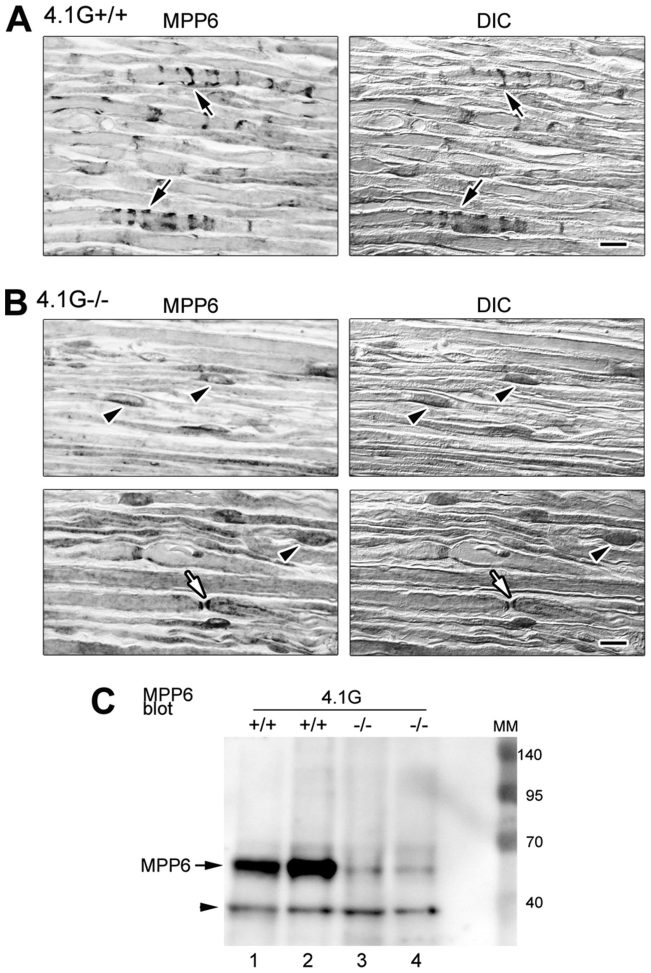

FIG 1 Immunolocalization of MPP6 in the $4.1G^{+/+}$ (A) and $4.1G^{-/-}$ (B) mouse sciatic nerves with the *in vivo* cryotechnique. The images on the right in panels A and B are differential interference contrast (DIC) images to demonstrate each nerve fiber. Although the MPP6 immunolocalization is obvious in SLI of the $4.1G^{+/+}$ nerves (arrows), it is only detected around the nuclei in the $4.1G^{-/-}$ nerves (arrowheads). The white arrows in panel B show the MPP6 immunolocalization in paranodes beside the node of Ranvier. (C) Immunoblotting for MPP6 lysates in the $4.1G^{+/+}$ (lanes 1 and 2) or $4.1G^{-/-}$ (lanes 3 and 4) mouse sciatic nerves. Two different mouse samples from each group are shown as examples. The intensity of the 55-kDa line (arrow) in the $4.1G^{-/-}$ mice was markedly reduced compared to that in the $4.1G^{+/+}$ mice. The arrowhead indicates a weaker blotted line (less than 30 kDa), probably due to an isoform or nonspecific reaction. MM, molecular marker. Bars, 10 μm.

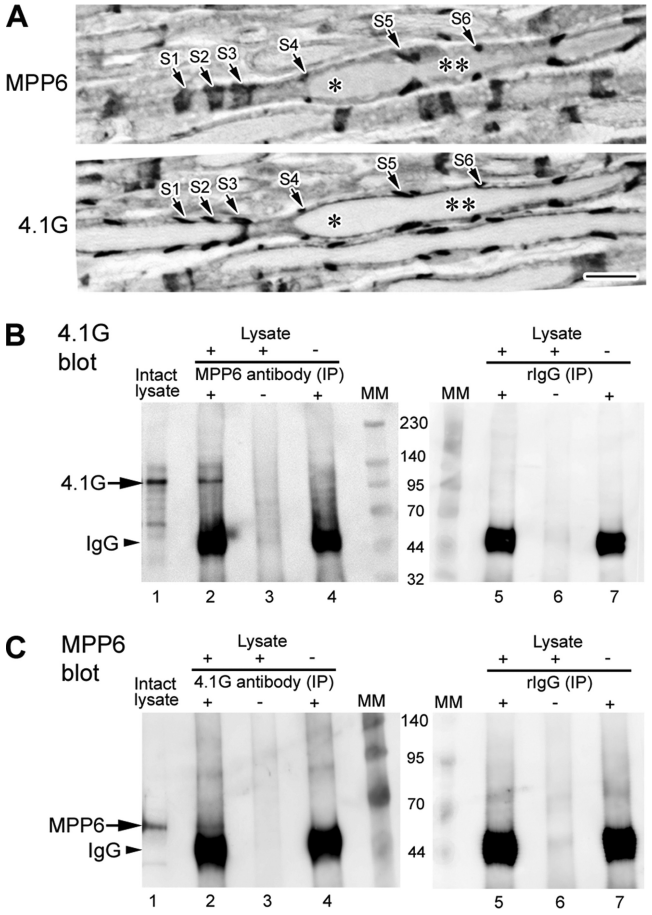

FIG 2 Immunolocalization of MPP6 and 4.1G in serial sections of mouse sciatic nerves with an *in vivo* cryotechnique (A) and immunoprecipitation (IP) study of the MPP6-4.1G interaction (B and C). (A) Arrows with S1 to S6 labels indicate SLI from the MPP6 (top) and 4.1G (bottom) immunostaining, and their immunolocalization in SLI largely matches. Bar, 20 μm. (B and C) Lanes 1 show the 4.1G (B) or MPP6 (C) immunoblotting of the intact sciatic nerve lysates. Lanes 2 to 7 show the 4.1G (B) or MPP6 (C) immunoblotting for three different samples as follows. Sciatic nerve lysates are included in the samples of lanes 2, 3, 5, and 6 but not in those of lanes 4 and 7, confirming that original mouse IgG was completely depleted by the Sepharose-G pretreatment. The MPP6 (B) or 4.1G (C) Ab is included in samples of lanes 2 and 4 for IP but not in that of lane 3, indicating that the 50-kDa line is derived from the anti-MPP6 (Fig. 2B) or anti-4.1G (Fig. 2C) antibody-derived IgG proteins (arrowheads in B and C; IgG). Arrows in B and C indicate the molecular masses of 4.1G (around 110 kDa) and MPP6 (around 55 kDa), respectively, and the lines at the same molecular masses in lane 2 but not in lanes 3 and 4, indicating the interaction of the proteins. Rabbit IgG (rIgG) is included in samples of lanes 5 and 7, but no 110-kDa (B) or 55-kDa (C) line appeared, indicating no reaction of rIgG to 4.1G or MPP6.

ment with data for our IVCT-FS samples, the disappearance of MPP6 from the SLI also was noted by CLSM ($4.1G^{-/-}$; top lane in Fig. 3A). Some undefined cells other than the myelinated nerve fibers also were immunostained with anti-MPP6 Ab in both $4.1G^{+/+}$ and $4.1G^{-/-}$ sciatic nerves (white arrowheads in Fig. 3A). Although the MPP6 immunolocalization was not observed in SLI of $4.1G^{-/-}$ nerve fibers, E-cadherin still was detected (middle lane in Fig. 3A). E-cadherin labeling also revealed that the shape of SLI in the $4.1G^{-/-}$ nerve fibers appeared different from that of wild-type nerves. To further examine this point, we measured the circular truncated cone heights of the SLI (Fig. 3B). The E-cadherin-positive SLI height in the $4.1G^{-/-}$ mice was statistically lower than that in wild-type animals (Fig. 3B).

Since E-cadherin labels adherens junctions that are present mostly at the outer edge of SLI (12, 43), we also used phalloidin to label filamentous actin that is present along the entire SLI structure (Fig. 3C). To evaluate the necessity of the freeze-thaw treatment for the teased sciatic nerves, heights of the circular truncated cones were measured for both E-cadherin immunostaining and phalloidin staining with or without the freeze-thaw treatment (Fig. 3C and D). To obtain strong phalloidin staining, Triton X-100 treatment was useful (data not shown). An example of the double-fluorescence staining is demonstrated in Fig. 3C. As previously reported (12, 43), E-cadherin immunoreactivity was restricted to the outer edge of the SLI either with or without the

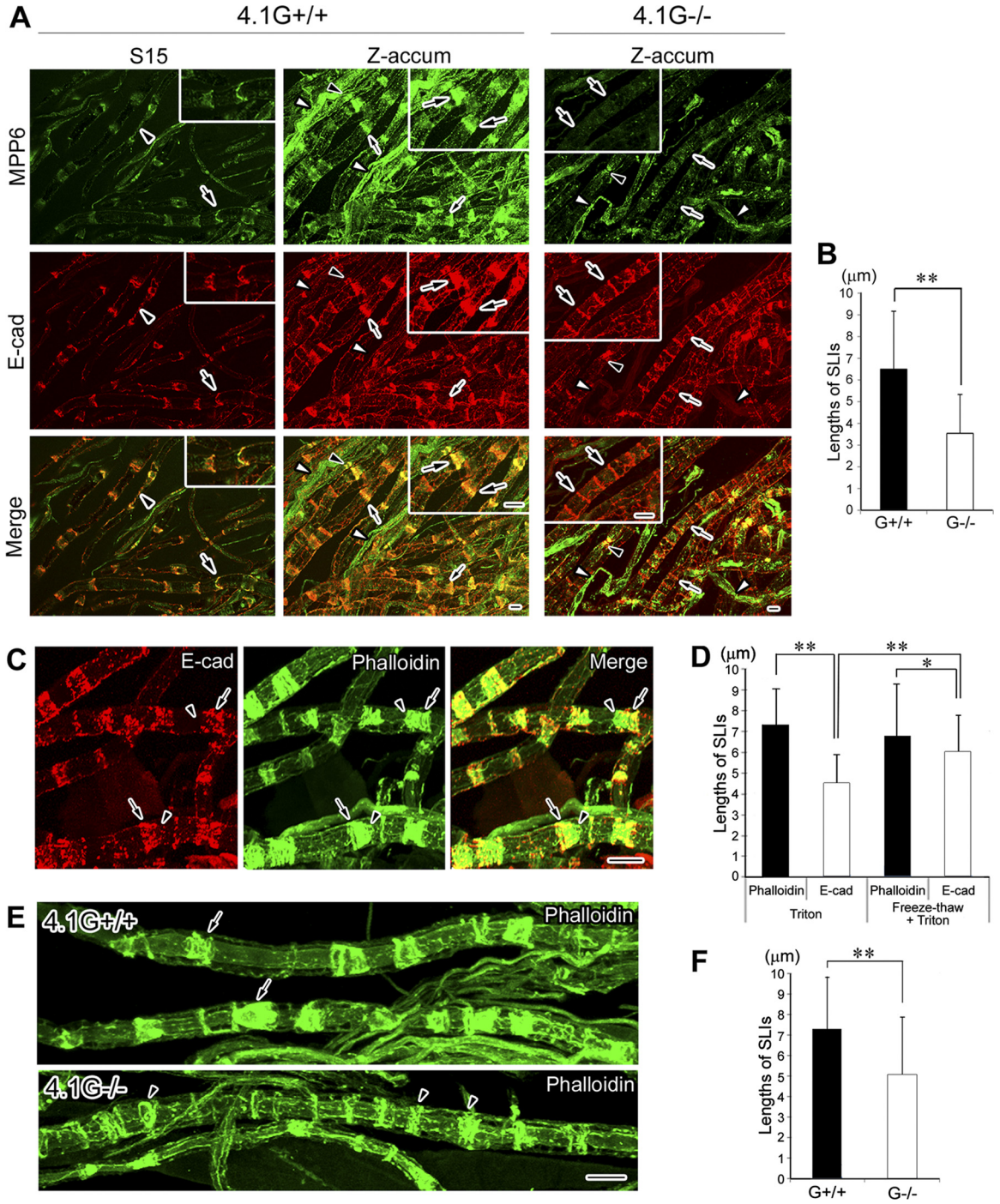

FIG 3 MPP6 and E-cadherin (E-cad) immunolocalization and phalloidin staining in 4.1G$^{+/+}$ and 4.1G$^{-/-}$ mouse-teased sciatic nerves. (A) CLSMs of MPP6 (green) and E-cad (red) immunostaining of the 15th optical section of 4.1G$^{+/+}$ mice (S15). Micrographs in the bottom lane show merged images of the two immunostainings, indicating the colocalization of 4.1G and E-cad in mesoaxons (arrowheads) and SLI (arrows). Insets show highly magnified views of parts of the SLI. Z-accum images show accumulated Z series from 70 optical sections (0.5 μm each) of the MPP6 (green), E-cad (red), and merged images in the 4.1G$^{+/+}$ and 4.1G$^{-/-}$ sciatic nerves. Insets show highly magnified views of parts of SLI. Note the disappearance of the MPP6 immunostaining in SLI of the 4.1G$^{-/-}$ sciatic nerves (arrows). Some cells other than myelinated nerve fibers are immunostained with the anti-MPP6 antibody (white arrowheads in 4.1G$^{+/+}$). (B) Statistical analysis for the heights of the circular truncated cones of SLI ($n = 600$) in sciatic nerves of three aged (10-month-old) 4.1G$^{+/+}$ and 4.1G$^{-/-}$ mice. The heights of the circular truncated cones of SLI in the 4.1G$^{-/-}$ nerves are lower than those in the 4.1G$^{+/+}$ ones. **, $P < 0.01$. (C) Example of a CLSM of the double staining for E-cad (red) and filamentous actin (phalloidin; green) and their merged image (merge) in the teased sciatic nerves with the freeze-thaw treatment. Although both E-cad and phalloidin staining colocalize at the outside edge of SLI (arrows), phalloidin staining is detected alone near the inner edge (arrowheads). (D) Statistical analysis for heights of the circular truncated cones of SLI ($n = 300$) in teased sciatic nerves with Triton X-100 treatment alone (Triton) or freeze-thaw treatment before the Triton treatment (Freeze-thaw + Triton). *, $P < 0.05$; **, $P < 0.01$. (E) Representative CLSM of teased sciatic nerves with phalloidin staining in 4.1G$^{+/+}$ or 4.1G$^{-/-}$ mice. The structure of the circular truncated cones of SLI in the 4.1G$^{-/-}$ nerve fibers (arrowheads) is different from that in 4.1G$^{+/+}$ ones (arrows). (F) Statistical analysis for heights of the circular truncated cones of SLI ($n = 600$) in teased sciatic nerves in three 4.1G$^{+/+}$ or 4.1G$^{-/-}$ mice. **, $P < 0.01$. Bars, 10 μm.

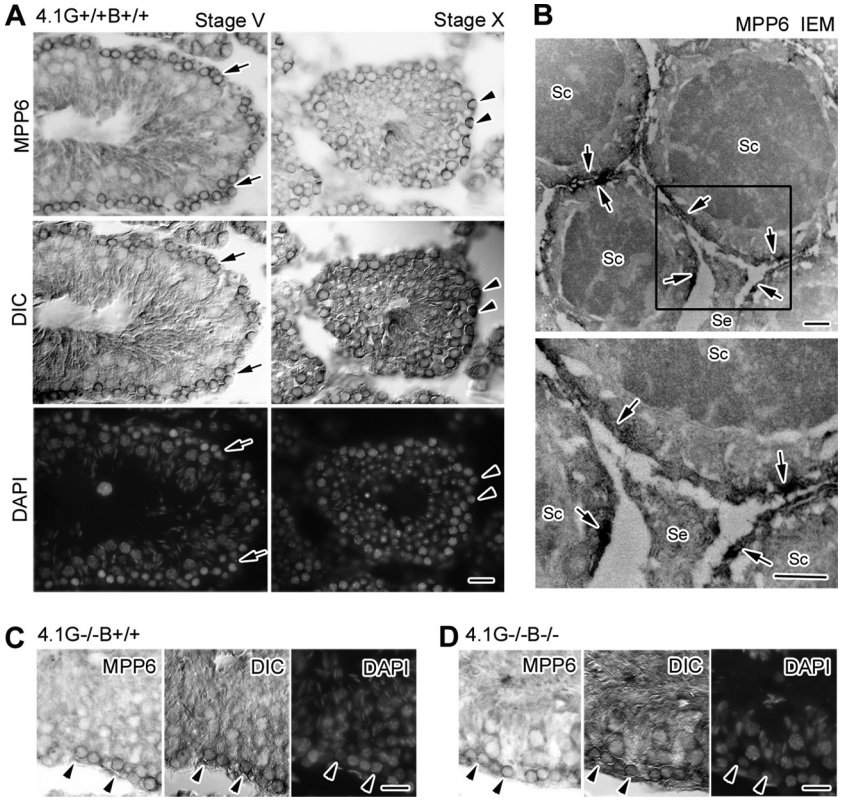

FIG 4 Immunostaining of MPP6 in seminiferous tubules for perfusion fixation followed by sucrose embedding for the $4.1G^{+/+}/B^{+/+}$ (A and B), $4.1G^{-/-}/B^{+/+}$ (C), and $4.1G^{-/-}/B^{-/-}$ (D) mice. (A) With light microscopic images, MPP6 is immunolocalized in germ cells in the basal parts of the seminiferous tubules at stages V (left) and X (right), indicating the spermatogonium and early spermatocytes. The intensity of the MPP6 immunostaining in the arch-shaped spermatogonium is obvious at stage X (arrowheads). (B) With immunoelectron microscopy, DAB reaction products with the anti-MPP6 antibody are detected (arrows) under cell membranes of spermatocytes (Sc). Se, Sertoli cell process. The bottom image shows a higher-magnification view of the rectangular part of the upper image. (C and D) In the $4.1G^{-/-}/B^{+/+}$ (C) and $4.1G^{-/-}/B^{-/-}$ (D) mice, MPP6 immunostaining was detected in the basal parts of the seminiferous tubules (arrowheads). Bars, 20 (A, C, and D) and 1 μm (B). DAPI, 4′,6′-diamidino-2-phenylindole; IEM, immunoelectron microscopy.

freeze-thaw treatment (Fig. 3C). In both cases, the heights of the circular truncated cones of E-cadherin labeling were lower than those measured after phalloidin staining (Fig. 3D). Without the freeze-thaw treatment, heights of the circular truncated cones with the E-cadherin immunostaining were lower than those with the treatment (Fig. 3D), indicating the usefulness of the freeze-thaw treatment for the E-cadherin immunostaining. As expected, for the phalloidin staining, the heights of the circular truncated cones without the freeze-thaw treatment were not different from those with the treatment (Fig. 3D). Accordingly, we measured the heights of the circular truncated cones in phalloidin-labeled nerves obtained from wild-type and $4.1G^{-/-}$ nerve fibers without the freeze-thaw treatment (Fig. 3E). The heights in $4.1G^{-/-}$ nerve fibers were significantly lower than those of the wild type (Fig. 3F). These results suggest that protein 4.1G is required for the assembly of the SLI.

Immunolocalization of MPP6 in the seminiferous tubules of $4.1G^{+/+}$ or $4.1G^{-/-}$ mice. Previous studies revealed that MPP6 mRNA and protein are detected in testes (44). Therefore, we examined the distribution of MPP6 in the mouse seminiferous tubules by immunohistochemistry (Fig. 4A and B). MPP6 was localized mainly at basal parts of the seminiferous tubules, where it was detected along cell membranes in the spermatogonium and early spermatocytes (Fig. 4A and B). This immunostaining pattern of MPP6 was similar to that of 4.1G, as we previously demonstrated (37).

We next determined whether the localization of MPP6 in the seminiferous tubules requires 4.1G. As depicted in Fig. 4C, MPP6 was detected along cell membranes of the germ cells in both wild-type and $4.1G^{-/-}$ mice. Given that protein 4.1B, another member of the 4.1 family, also is found in the rodent seminiferous tubules (39), we examined the localization of MPP6 in mutant mice that lack both protein 4.1B and 4.1G (Fig. 4D). MPP6 immunoreactivity in germ cells was indistinguishable between 4.1B/G double mutant mice and wild-type mice, indicating that in contrast to myelinating Schwann cells, the localization of MPP6 in the seminiferous tubules does not require 4.1G.

DISCUSSION

In this study, we found that 4.1G interacts with MPP6 and is required for the latter's targeting to cell membranes of the SLI in myelinating Schwann cells. In contrast, although MPP6 was detected in germ cells of mouse seminiferous tubules, especially in the spermatogonium and early spermatocytes, its localization in this tissue is independent of the presence of either 4.1G or 4.1B. This indicates that spermatogenic germ cells have a different mechanism for the targeting of MPP6 to cell membranes than the Schwann cells.

MPP6 originally was identified in epithelial cells as a mammalian homologue of Lin-7 (mLin-7)-binding protein (15, 44) and is thought to play a role in the targeting of proteins to basolateral surfaces. Although MPP6 was previously shown not to interact with 4.1R (44), we demonstrate that it interacts with 4.1G in myelinating Schwann cells. The existence of an MPP6-4.1G complex in mouse Schwann cells is analogous to the MPP1 (p55)-4.1R complex found in erythrocytes (22, 29, 33), CASK-4.1N interaction in neurons (3), and MPP6-4.1B interaction in epithelial cells (34). In the $4.1G^{-/-}$ mouse sciatic nerves, the total amount of MPP6 was significantly reduced and the protein was detected in the cytoplasm near the Schwann cell nuclei, which is abnormal. Nevertheless, MPP6 still was present at the paranodal loops even in the $4.1G^{-/-}$ sciatic nerves, indicating the independency of 4.1G in the MPP6 targeting to paranodes. MAGUK proteins are thought to function as scaffolding for cargoes and interact with motor molecules on microtubules (45). One of the ezrin-radixin-moesin (ERM)-containing proteins, merlin, was reported to directly interact with both microtubules (48) and kinesin motor proteins (2). Although merlin also was reported to be expressed in Schwann cells (32), our results indicate that it is not related to the MPP6 targeting to SLI. However, a future temporal and spatial study of an ERM protein, such as merlin, and 4.1G-MPP6 on microtubules will be interesting.

It is interesting that the size of SLI in the aged $4.1G^{-/-}$ mice was different from that in wild-type mice, as revealed by both E-cadherin and actin staining. A MAGUK, MPP5 (Pals1), was reported to regulate the E-cadherin trafficking in mammalian epithelial cells (47). On the other hand, another 4.1 family protein, 4.1R, was shown to link to E-cadherin/β-catenin in mouse stomach epithelial cells (50). We believe that the MPP6-4.1G complex affects the maintenance of the SLI structure during aging. It is well known that 4.1R-deficient erythrocytes become elliptocytes from normal biconcave discs, depending on the age of the erythrocytes, due to the gradual instability of functional membrane skeletons to resist mechanical strength under circulation (19). As the lengths of peripheral nervous system (PNS) nerve fibers easily change with mechanical stretching in animal bodies during exercise, it is possible that the SLI present along myelin internodes in the PNS have a role in protecting peripheral nerves during mechanical external forces. For the specific membrane adhesion structure in internodes, SLI have various tight and adherens junctional molecules (28), such as claudin (28), occludin (1), E-cadherin (43, 51), and junctional adhesion molecule C (JAM-C) (31). In this paper, we demonstrated that the MPP6-4.1G complex has a functional role in the long-term maintenance of the SLI structures. Because spectrin-actin (35) and MPP6-4.1G are localized in SLI, a more precise ultrastructural study will be needed to reveal the functional mechanism of the membrane skeletons at this location.

A further question is what would happen if MPP6 is deficient for 4.1G targeting as well as for SLI formation? The requirement of MPP6 was reported for the maturation and function of *Drosophila* septate junctions (20). In addition, other MAGUKs, such as Dlg1 (5, 6, 8, 13) and MPP5 (25), were reported to affect myelination if they were deficient due to the disruption of the phosphatidylinositol metabolism with Mtmr-2 (myotubularin-related 2) and PTEN (phosphatase and tensin homolog). On the other hand, it has been demonstrated that MAGUK family members, such as Dlg1 and MPP7, interact with each other in epithelial cells (4). Therefore, the examination of the relationships between MPP6 and MPP5 in Schwann cells will be needed.

In addition, the dependence of MPP6 on the formation of mammalian seminiferous tubules is another concern, because Dlg was reported to function in gamete development in *Drosophila* testes (26). Compared to the Schwann cells, it is interesting that the disappearance of the MPP6 targeting was not detected in the testicular germ cells in $4.1G^{-/-}$ and $4.1B^{-/-}$ mice, as shown in Fig. 4C and D. It is important to examine the mechanism of the 4.1G targeting of MPP6 to solve the question of why such different events happened in different organs.

ACKNOWLEDGMENTS

This work was partially supported by a grant from the Japanese Society for the Promotion of Science (KAKEN number 21590214) to N. Terada and the National Institutes of Health (NS50220) to E. Peles.

We thank Yutaka Kitahara in the Department of Anatomy and Molecular Histology, Interdisciplinary Graduate School of Medicine and Engineering, University of Yamanashi, for his technical assistance.

REFERENCES

1. **Alanne MH, et al.** 2009. Tight junction proteins in human Schwann cell autotypic junctions. J. Histochem. Cytochem. **57**:523–529.
2. **Benseñor LB, Barlan K, Rice SE, Fehon RG, Gelfand VI.** 2010. Microtubule-mediated transport of the tumor-suppressor protein Merlin and its mutants. Proc. Natl. Acad. Sci. U. S. A. **107**:7311–7316.
3. **Biederer T, Sudhof TC.** 2001. CASK and protein 4.1 support F-actin nucleation on neurexins. J. Biol. Chem. **276**:47869–47876.
4. **Bohl J, Brimer N, Lyons C, Vande Pol SB.** 2007. The stardust family protein MPP7 forms a tripartite complex with LIN7 and DLG1 that regulates the stability and localization of DLG1 to cell junctions. J. Biol. Chem. **282**:9392–9400.
5. **Bolino A, et al.** 2004. Disruption of Mtmr2 produces CMT4B1-like neuropathy with myelin outfolding and impaired spermatogenesis. J. Cell Biol. **167**:711–721.
6. **Bolis A, et al.** 2009. Dlg1, Sec8, and Mtmr2 regulate membrane homeostasis in Schwann cell myelination. J. Neurosci. **29**:8858–8870.
7. **Chen J, et al.** 2011. Immunolocalization of membrane skeletal protein, 4.1G, in enteric glial cells in the mouse large intestine. Neurosci. Lett. **488**:193–198.
8. **Cotter L, et al.** 2010. Dlg1-PTEN interaction regulates myelin thickness to prevent damaging peripheral nerve overmyelination. Science **328**: 1415–1418.
9. **de Mendoza A, Suga H, Ruiz-Trillo I.** 2010. Evolution of the MAGUK protein gene family in premetazoan lineages. BMC Evol. Biol. **10**:93.
10. **Discher DE, et al.** 1995. Mechanochemistry of protein 4.1's spectrin-actin-binding domain: ternary complex interactions, membrane binding, network integration, structural strengthening. J. Cell Biol. **130**:897–907.
11. **Funke L, Dakoji S, Bredt DS.** 2005. Membrane-associated guanylate kinases regulate adhesion and plasticity at cell junctions. Annu. Rev. Biochem. **74**:219–245.
12. **Ghabriel MN, Allt G.** 1981. Incisures of Schmidt-Lanterman. Prog. Neurobiol. **17**:25–58.
13. **Goebbels S, et al.** 2010. Elevated phosphatidylinositol 3,4,5-trisphosphate in glia triggers cell-autonomous membrane wrapping and myelination. J. Neurosci. **30**:8953–8964.
14. **Hanada T, Takeuchi A, Sondarva G, Chishti AH.** 2003. Protein 4.1-mediated membrane targeting of human discs large in epithelial cells. J. Biol. Chem. **278**:34445–34450.
15. **Kamberov E, et al.** 2000. Molecular cloning and characterization of Pals, proteins associated with mLin-7. J. Biol. Chem. **275**:11425–11431.
16. **Lozovatsky L, Abayasekara N, Piawah S, Walther Z.** 2009. CASK deletion in intestinal epithelia causes mislocalization of LIN7C and the DLG1/Scrib polarity complex without affecting cell polarity. Mol. Biol. Cell **20**: 4489–4499.
17. **Lue RA, Brandin E, Chan EP, Branton D.** 1996. Two independent domains of hDlg are sufficient for subcellular targeting: the PDZ1-2 conformational unit and an alternatively spliced domain. J. Cell Biol. **135**: 1125–1137.

18. **Lue RA, Marfatia SM, Branton D, Chishti AH.** 1994. Cloning and characterization of hdlg: the human homologue of the Drosophila discs large tumor suppressor binds to protein 4.1. Proc. Natl. Acad. Sci. U. S. A. **91**:9818–9822.
19. **Mohandas N, Gallagher PG.** 2008. Red cell membrane: past, present, and future. Blood **112**:3939–3948.
20. **Moyer KE, Jacobs JR.** 2008. Varicose: a MAGUK required for the maturation and function of Drosophila septate junctions. BMC Dev. Biol. **8**:99.
21. **Nix SL, Chishti AH, Anderson JM, Walther Z.** 2000. hCASK and hDlg associate in epithelia, and their src homology 3 and guanylate kinase domains participate in both intramolecular and intermolecular interactions. J. Biol. Chem. **275**:41192–41200.
22. **Nunomura W, Takakuwa Y, Parra M, Conboy J, Mohandas N.** 2000. Regulation of protein 4.1R, p55, and glycophorin C ternary complex in human erythrocyte membrane. J. Biol. Chem. **275**:24540–24546.
23. **Ohno N, et al.** 2009. Dispensable role of protein 4.1B/DAL-1 in rodent adrenal medulla regarding generation of pheochromocytoma and plasmalemmal localization of TSLC1. Biochim. Biophys. Acta **1793**:506–515.
24. **Ohno N, et al.** 2006. Expression of protein 4.1G in Schwann cells of the peripheral nervous system. J. Neurosci. Res. **84**:568–577.
25. **Ozçelik M, et al.** 2010. Pals1 is a major regulator of the epithelial-like polarization and the extension of the myelin sheath in peripheral nerves. J. Neurosci. **30**:4120–4131.
26. **Papagiannouli F, Mechler BM.** 2009. Discs large regulates somatic cyst cell survival and expansion in Drosophila testis. Cell Res. **19**:1139–1149.
27. **Parra M, et al.** 1998. Cloning and characterization of 4.1G (EPB41L2), a new member of the skeletal protein 4.1 (EPB41) gene family. Genomics **49**:298–306.
28. **Poliak S, Matlis S, Ullmer C, Scherer SS, Peles E.** 2002. Distinct claudins and associated PDZ proteins form different autotypic tight junctions in myelinating Schwann cells. J. Cell Biol. **159**:361–372.
29. **Quinn BJ, et al.** 2009. Erythrocyte scaffolding protein p55/MPP1 functions as an essential regulator of neutrophil polarity. Proc. Natl. Acad. Sci. U. S. A. **106**:19842–19847.
30. **Saitoh Y, et al.** 2010. Histochemical approach of cryobiopsy for glycogen distribution in living mouse livers under fasting and local circulation loss conditions. Histochem. Cell Biol. **133**:229–239.
31. **Scheiermann C, et al.** 2007. Expression and function of junctional adhesion molecule-C in myelinated peripheral nerves. Science **318**:1472–1475.
32. **Scherer SS, Gutmann DH.** 1996. Expression of the neurofibromatosis 2 tumor suppressor gene product, merlin, in Schwann cells. J. Neurosci. Res. **46**:595–605.
33. **Seo PS, et al.** 2009. Alternatively spliced exon 5 of the FERM domain of protein 4.1R encodes a novel binding site for erythrocyte p55 and is critical for membrane targeting in epithelial cells. Biochim. Biophys. Acta **1793**: 281–289.
34. **Shingai T, et al.** 2003. Implications of nectin-like molecule-2/IGSF4/RA175/SgIGSF/TSLC1/SynCAM1 in cell-cell adhesion and transmembrane protein localization in epithelial cells. J. Biol. Chem. **278**: 35421–35427.
35. **Susuki K, et al.** 2011. Schwann cell spectrins modulate peripheral nerve myelination. Proc. Natl. Acad. Sci. U. S. A. **108**:8009–8014.
36. **Terada N, et al.** 2009. Involvement of dynamin-2 in formation of discoid vesicles in urinary bladder umbrella cells. Cell Tissue Res. **337**:91–102.
37. **Terada N, et al.** 2010. Involvement of a membrane skeletal protein, 4.1G, for Sertoli/germ cell interaction. Reproduction **139**:883–892.
38. **Terada N, Ohno N, Saitoh S, Saitoh Y, Ohno S.** 2009. Immunoreactivity of glutamate in mouse retina inner segment of photoreceptors with in vivo cryotechnique. J. Histochem. Cytochem. **57**:883–888.
39. **Terada N, et al.** 2004. Immunohistochemical study of protein 4.1B in the normal and W/W (v) mouse seminiferous epithelium. J. Histochem. Cytochem. **52**:769–777.
40. **Terada N, et al.** 2005. Immunohistochemical study of a membrane skeletal molecule, protein 4.1G, in mouse seminiferous tubules. Histochem. Cell Biol. **124**:303–311.
41. **Terada N, et al.** 2010. Visualization of microvascular blood flow in mouse kidney and spleen by quantum dot injection with "in vivo cryotechnique." Microvasc. Res. **80**:491–498.
42. **Trapp BD, Andrews SB, Wong A, O'Connell M, Griffin JW.** 1989. Co-localization of the myelin-associated glycoprotein and the microfilament components, F-actin and spectrin, in Schwann cells of myelinated nerve fibres. J. Neurocytol. **18**:47–60.
43. **Tricaud N, Perrin-Tricaud C, Bruses JL, Rutishauser U.** 2005. Adherens junctions in myelinating Schwann cells stabilize Schmidt-Lanterman incisures via recruitment of p120 catenin to E-cadherin. J. Neurosci. **25**: 3259–3269.
44. **Tseng TC, et al.** 2001. VAM-1: a new member of the MAGUK family binds to human Veli-1 through a conserved domain. Biochim. Biophys. Acta **1518**:249–259.
45. **Verhey KJ, Rapoport TA.** 2001. Kinesin carries the signal. Trends Biochem. Sci. **26**:545–550.
46. **Walensky LD, et al.** 1998. The 13-kD FK506 binding protein, FKBP13, interacts with a novel homologue of the erythrocyte membrane cytoskeletal protein 4.1. J. Cell Biol. **141**:143–153.
47. **Wang Q, Chen XW, Margolis B.** 2007. PALS1 regulates E-cadherin trafficking in mammalian epithelial cells. Mol. Biol. Cell **18**:874–885.
48. **Xu HM, Gutmann DH.** 1998. Merlin differentially associates with the microtubule and actin cytoskeleton. J. Neurosci. Res. **51**:403–415.
49. **Yamada KH, Hanada T, Chishti AH.** 2007. The effector domain of human Dlg tumor suppressor acts as a switch that relieves autoinhibition of kinesin-3 motor GAKIN/KIF13B. Biochemistry **46**:10039–10045.
50. **Yang S, Guo X, Debnath G, Mohandas N, An X.** 2009. Protein 4.1R links E-cadherin/beta-catenin complex to the cytoskeleton through its direct interaction with beta-catenin and modulates adherens junction integrity. Biochim. Biophys. Acta **1788**:1458–1465.
51. **Young P, et al.** 2002. E-cadherin is required for the correct formation of autotypic adherens junctions of the outer mesaxon but not for the integrity of myelinated fibers of peripheral nerves. Mol. Cell Neurosci. **21**: 341–351.